DOI: 10.1002/ejic.200800031

# Extended Networks Generated from the Interaction of Rare-Earth(III) Ions and Pyridine-2-carboxamide-Based Ligands

**Maarten G. van der Horst,[a] Gerard A. van Albada,[a] Rodica-Mariana Ion,[b] Ilpo Mutikainen,[c] Urho Turpeinen,[c] Stefania Tanase,*[a] and Jan Reedijk[a]**

**Keywords:** Rare earths / Crystal structure / Bridging ligands / Magnetic properties / Luminescence

The reaction of the ligand 1,4-bis(pyridine-2-carboxamido)-butane (L) with $RECl_3$ afforded complexes of general formula $[RE(L)_{1.5}Cl_2(CH_3OH)]Cl{\cdot}nS$ (RE = Pr, Nd, Eu, Tb; $n$ = 4, S = $H_2O$; $n$ = 5, S = $CH_3OH$). The structural determination reveals that complexes $[RE(L)_{1.5}Cl_2(CH_3OH)]Cl{\cdot}5CH_3OH$ (RE = Nd **2b**, Eu **3b**) are isomorphous, crystallizing in the monoclinic system, space group $P2_1/n$; they possess a 2D architecture with the rare-earth ion in an eight-coordination geometry. By exposure to air, the lattice methanol molecules are easily replaced by water molecules to form the analogues $[RE(L)_{1.5}Cl_2(CH_3OH)]Cl{\cdot}4H_2O$ (RE = Pr **1**, Nd **2a**, Eu **3a**, Tb **4**) as indicated by elemental analysis, IR, and thermogravimetric analysis. Photophysical studies on the $Eu^{III}$ and $Tb^{III}$ complexes showed that excitation into the ligand-centered $\pi\rightarrow\pi^*$ transition results in the characteristic visible luminescence from $Eu^{III}$ at 614 nm and $Tb^{III}$ at 545 nm. The magnetic properties were also investigated and show that crystal field effects are dominant.


## Introduction

Rare-earth polynuclear complexes offer attractive properties in terms of their potential applications as luminescent, nonlinear optical, magnetic, and porous materials.[1–7] Interest in such materials begun in 1999 when Yaghi and coworkers reported that the self-assembly of $Tb(NO_3)_3$ and 1,4-benzenedicarboxylate afforded zeolite-like frameworks that are capable of reversible molecular sorption and of maintaining microporosity in the absence of included guests.[8] Since then, various carboxylate anions with aromatic rings have been widely employed to construct coordination polymers containing rare-earth (RE) ions.[9–21] However, the synthesis of such materials is carried out in aqueous media where water molecules coordinate easily to the rare-earth(III) ion and this usually quenches the emission intensity. Nevertheless, the unpredictable nature and lability of the rare-earth ions led to both exciting opportunities and to difficulties in targeted materials synthesis. Champness and coworkers discovered that 4,4′-bipyridine *N*,*N*′-dioxide possess an excellent hard acid/hard base complementarity of the rare-earth ions and the *N*-oxide donor as well as a small steric size that avoids crowding at the metal center.[22–26] As a result of the tendency of rare-earth metals to adopt high coordination numbers and their ability to adapt to a given environment, highly connected frameworks have been obtained.[22–26]

To build a coordination network, the coordinative-bond approach is the most appropriate one. It is also possible, even in parallel, to use highly directional hydrogen bonds as a means of controlling self-assembly in supramolecular systems. Although hydrogen bonding has been widely used to construct supramolecular assemblies,[27,28] strategies for their inclusion in assembling rare-earth coordination polymers have remained unexplored. In this respect, amide-based ligands are attractive bifunctional units capable of binding a rare-earth ion while retaining a face capable of hydrogen bonding interactions. A few recent reports have shown that 1D coordination polymers containing pyrazol–pyridine amide units connected to a central spacer,[29] 2D extended networks with channel structures from a cyclic amide,[30] and metallodendrimers from tripodal amide ligands[31] can indeed be obtained. As a part of our research aimed at the design of luminescent rare-earth complexes based on pyridine-2-carboxamide units,[32] we employed the 1,4-bis(pyridine-2-carboxamido)butane ligand (L, Figure 1) as a flexible coordination unit to form coordination polymers. In the present contribution, we report on the synthesis, crystal structure, and properties of a series of isostructural 2D extended networks of general formula $[RE(L)_{1.5}Cl_2(CH_3OH)]Cl{\cdot}nS$ (RE = Pr, Nd, Eu, Tb; $n$ = 4, S = $H_2O$; $n$ = 5, S = $CH_3OH$).

[a] Leiden Institute of Chemistry, Gorlaeus Laboratories, Leiden University,
P. O. Box 9502, 2300 RA Leiden, The Netherlands
Fax: +31-71-5274451
E-mail: s.grecea@chem.leidenuniv.nl
[b] National Institute for Chemical and Petrochemical Research, Splaiul Independentei 202, 060021 Bucharest, Romania
[c] Laboratory of Inorganic Chemistry, Department of Chemistry, University of Helsinki,
P. O. Box 55, (A. I. Virtasen aukio 1), 00014 Helsinki, Finland
Supporting information for this article is available on the WWW under http://www.eurjic.org/ or from the author.

  

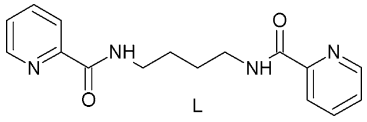


Figure 1. Ligand 1,4-bis(pyridine-2-carboxamido)butane.

## Results and Discussion

### Synthesis and Characterization

Complexes $[RE(L)_{1.5}Cl_2(CH_3OH)]Cl{\cdot}5CH_3OH$ (RE = Nd **2b**, Eu **3b**) were obtained by reaction of $RECl_3$ with the neutral donor ligand 1,4-bis(pyridine-2-carboxamido)butane (L) in a 1:1.5 ratio in methanol. Slow diffusion of diisopropyl ether into the methanol solution afforded single crystals suitable for X-ray analysis, and the crystal structure is described below. The crystallinity of the compounds is lost upon removing the crystals from the mother liquid and the five guest methanol molecules are easily replaced by four water molecules as indicated by elemental, IR spectroscopic, and thermogravimetric analysis. Nevertheless, the $[RE(L)_{1.5}Cl_2(CH_3OH)]Cl{\cdot}4H_2O$ (RE = Pr **1**, Nd **2a**, Eu **3a**, Tb **4**) analogues can be obtained in good yields by slow diffusion of diethyl ether into the methanol solution, followed by filtration and drying in air of the crystalline material formed. It is possible to obtain the highly hydrated complexes $[RE(L)_{1.5}Cl_2(CH_3OH)]Cl{\cdot}8H_2O$ (RE = La, Pr, Nd, Sm, Eu, Tb) by the addition of ethyl acetate to the methanol solution. Attempts to isolate complexes of heavy rare-earth(III) ions were not successful. Apparently, their smaller size is responsible for some difficulties in the packing of relatively large ligand molecules in the first coordination sphere.

Complexes **1**, **2a**, **3a**, and **4** were obtained in good yields (up to 58%) and they are very stable when exposed to air. Therefore, all spectroscopic and magnetic studies were performed by using these compounds. The IR spectra of **1**, **2a**, **3a**, and **4** are identical. This suggests that the four complexes are isostructural. The intense band at ca. 1627 $cm^{-1}$ is assigned to the carbonyl group ($\nu_{C=O}$). The four C–H aromatic groups generate a characteristic symmetric out-of-plane bending at 754 $cm^{-1}$. The broad band in the range 3100–3300 $cm^{-1}$ occurs from the stretching vibrations of the lattice water molecules ($\nu_{O-H}$); the absence of a band at 590 $cm^{-1}$ shows that the water molecules in complexes **1**, **2a**, **3a**, and **4** are not coordinated water.[33]

### Description of the Crystal Structure

Complexes **2b** and **3b** are isostructural and crystallize in the space group $P2_1/n$ as 2D infinite network towards the *b* and *c* axis of the unit cell (Figure 2). Relevant bond lengths and angles are given in Table 1. Figure 3 shows the coordination geometry of $Nd^{III}$ in **2b**. Because the ionic radius of $Nd^{III}$ is slightly larger than that of the $Eu^{III}$ ion, all metal–ligand bonds in **2b** are longer than the corresponding bonds in **3b** (Table 1). However, the bond angles are nearly the same for **2b** and **3b**. The rare-earth(III) ion is surrounded by three amide groups from three ligands, which function as bridges. The coordination geometry is completed by two chlorido anions and one methanol molecule. The rare-earth to oxygen bond lengths are in the range 2.423(4)–2.472(4) Å for **2b** and 2.369(4)–2.402(4) Å for **3b**. The coordinated methanol is involved in a strong hydrogen bond with one of the methanol lattice molecules [**2b**: O1–H1···O2 2.667(8) Å; **3b**: O1–H1···O2 2.650(9) Å]. The two coordinated chlorido ions participate in hydrogen bonding with the neighboring amide groups [**2b**: N19–H19a···Cl1 3.175(6) Å, N29–H29a···Cl2 3.236(6) Å; **3b**: N19–H19a···Cl1 3.142(6) Å, N29–H29a···Cl2 3.196(6) Å]; one of them is also hydrogen bonded to a lattice methanol molecule [**2b**: O5–H5···Cl2 3.212(18) Å; **3b**: O5–H5···Cl2 3.150(18) Å]. In both complexes, the amide linkages are essentially planar [average dihedral angle for C–N(H)–C(=O)–C is 4.23° for **2b** and 4.19° for **3b**]. As a result of the conformation of the butylene bridge, the two carbonyl groups of each ligand are in an *anti* orientation, which facilitates the formation of an extended structure. The Nd···Nd separation is 12.295 Å along the *b* axis and 11.576 Å along the *c* axis. For **3b**, the Eu···Eu distances are 12.166 and 11.472 Å, respectively. In the cavities formed, free counter chloride ions and methanol molecules exist. The free chloride ion is involved in hydrogen bonding with two lattice methanol molecules [**2b**: O3–H3···Cl3 3.125(9) Å; O4–H4···Cl3 3.122(9) Å; **3b**: O3–H3···Cl3 3.112(9) Å; O4–H4···Cl3 3.093(9) Å] and an amide N–H group [**2b**: N39–H39a···Cl3 3.185(6) Å; **3b**: N39–H39a···Cl3 3.170(6) Å].

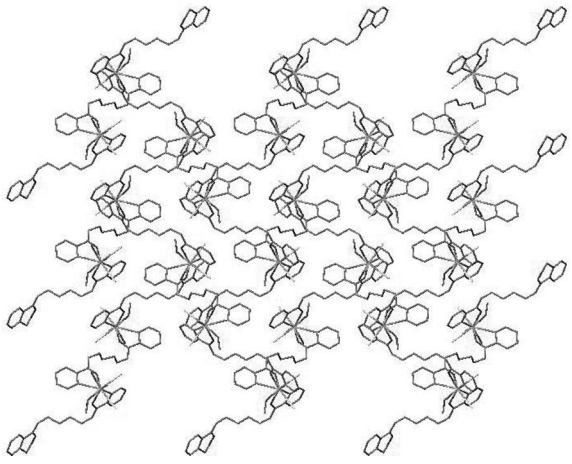

Figure 2. View of the two-dimensional network of **2b**. Noncoordinated chloride anion and the lattice methanol molecules are omitted for clarity.

  

Table 1. Selected bond lengths [Å] and angles [°] for **2b** and **3b**.[a]

| Bond lengths | | Bond angles | |
|---|---|---|---|
| **2b** | | | |
| Nd–Cl1 | 2.8118(18) | Cl1–Nd–Cl2 | 88.50(6) |
| Nd–Cl2 | 2.8692(19) | Cl1–Nd–O1 | 80.39(13) |
| Nd–O1 | 2.462(6) | Cl2–Nd–O38 | 76.20(12) |
| Nd–O18 | 2.454(4) | Cl2–Nd–O1 | 140.76(14) |
| Nd–O28d | 2.470(4) | O1–Nd–O18 | 75.82(17) |
| Nd–O38 | 2.422(6) | O1–Nd–O38 | 132.73(17) |
| Nd–N11 | 2.773(6) | O1–Nd–N31 | 72.92(19) |
| Nd–N21d | 2.775(6) | O18–Nd–N11 | 61.26(16) |
| Nd–N31 | 2.785(6) | O18–Nd–N31 | 69.10(16) |
| **3b** | | | |
| Eu–Cl1 | 2.7628(19) | Cl1–Eu–Cl2 | 88.01(6) |
| Eu–Cl2 | 2.828(2) | Cl1–Eu–O1 | 81.23(15) |
| Eu–O1 | 2.399(6) | Cl2–Eu–O38 | 139.93(13) |
| Eu–O18 | 2.395(4) | Cl2–Eu–O1 | 140.14(15) |
| Eu–O28d | 2.397(4) | O1–Eu–O18 | 75.44(18) |
| Eu–O38 | 2.371(6) | O1–Eu–O38 | 133.14(18) |
| Eu–N11 | 2.713(6) | O1–Eu–N31 | 72.70(19) |
| Eu–N21d | 2.722(6) | O18–Eu–N11 | 62.54(16) |
| Eu–N31 | 2.759(6) | O18–Eu–N31 | 68.52(16) |

[a] Symmetry operations: *x*, *y*, *z*; 1/2 – *x*, 1/2 + *y*, 1/2 –*z*; –*x*, –*y*, –*z*; 1/2 + *x*, 1/2 –*y*, 1/2 –*z*.

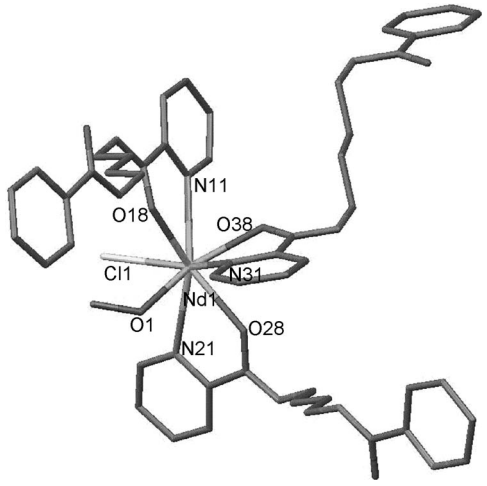


Figure 3. Coordination geometry of the $Nd^{III}$ ion in the molecular structure of **2b**. Hydrogen atoms are omitted for clarity.

## Thermal Gravimetric Analysis and Differential Thermal Analysis

TGA–DTA studies were performed in detail for complexes **1** and **2a**. Compounds **1** and **2a** exhibited similar mass losses over the entire operating range. In the case of **1**, initial loss of the lattice water is seen up to 200 °C and an advanced degradation process starting after 250 °C is observed (Figure 4).

For **2a**, the first decomposition stage, between 20 and 120 °C, starts with the loss of water. According to Figure 4, a strong degradation starts at about 294 °C. At this temperature, the weight loss exceeds 60%. For both compounds, the observed weight loss of water molecules is in agreement with that calculated for the crystal structure. The TGA weight-loss profile was mathematically deconvoluted

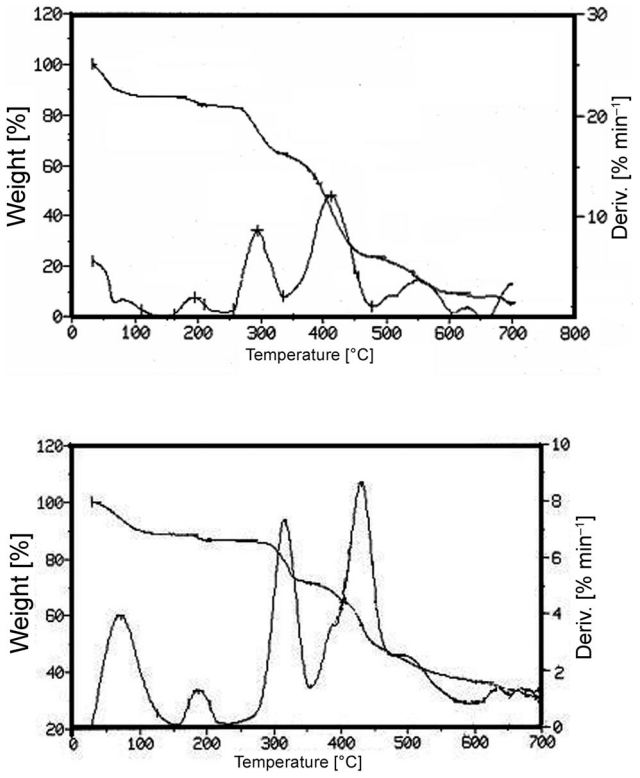


Figure 4. TGA analysis of **1** (top) and **2a** (bottom) over the temperature range from 30 to 800 °C at a heating rate of $\beta$ = 5 °C min$^{-1}$.

into six substages and each substage could be properly assigned to dehydration, concomitant dehydration and denitration, decarbonylation, followed by denitration and decomposition of residual compound. The degradation stages and the weight loss of **1** and **2a** are given in Tables S1 and S2 (Supporting Information).

## Spectroscopic Studies

The UV/Vis/NIR absorption properties of complexes **1**, **2a**, **3a**, and **4** were studied in the solid state; the absorption spectra of the ligand and complexes **1** and **2a** are shown in Figure 5. The free ligand L exhibits absorption bands at 267 and 303 nm; these bands are redshifted upon coordination to the rare-earth(III) ions. For **1**, the multiplet typical for $Pr^{III}$ corresponds to the transitions from the ground $^3H_4$ state to $^3P_2$ (455 nm), $^1I_6$+$^3P_1$ (478 nm), $^3P_0$ (493 nm), and $^1D_2$ (604 nm) levels.[34] These lines are strong and narrow and their shape suggests the appearance of $Pr^{III}$ in the single crystallographic site. The absorption spectrum of the $Nd^{III}$ ion is rich in bands in the visible and near-infrared region. These bands are caused by the transitions from the ground $^4I_{9/2}$ level to the excited *J* levels of $4f^3$ configuration. The excited levels of the visible- and near-ultraviolet bands are primarily determined by interelectronic repulsion parameters and to a smaller extent by the spin-orbit coupling, whereas the levels producing bands in the infrared, which

  

are essentially the members of the ground term, are separated by multiples. The most important observed peaks for **2a** correspond to the following transitions: 532 ($^4I_{9/2}\rightarrow{}^2K_{13/2}$, $^4G_{7/2}$, $^4G_{9/2}$), 587 ($^4I_{9/2}\rightarrow{}^4G_{5/2}$, $^2G_{7/2}$), 688 ($^4I_{9/2}\rightarrow{}^4F_{9/2}$), 751 ($^4I_{9/2}\rightarrow{}^4F_{7/2}$, $^4S^{3/2}$), 808 ($^4I_{9/2}\rightarrow{}^2H_{9/2}$, $^4F_{5/2}$), 892 nm ($^4I_{9/2}\rightarrow{}^4F_{3/2}$).[35]

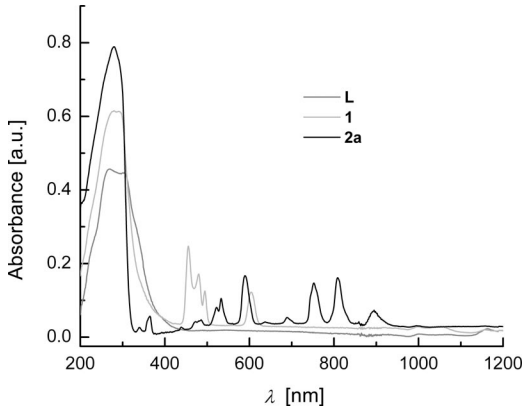


Figure 5. The absorption spectra of ligand L and that of complexes **1** and **2a**.

Emission spectra of complexes **3a** and **4** were measured at room temperature on solid samples. Upon excitation of the ligand-centered absorption bands, complex **3a** shows typical visible emission bands of the $Eu^{III}$ ion, which arise principally from transitions originating at the $^5D_0$ level (Figure 6). The strongest emission located around 614 nm is assigned to the $^5D_0\rightarrow{}^7F_2$ transition, which is an electric-dipole transition; it is sensitive to the symmetry of the coordination sphere and therefore is called *hypersensitive*. The $^5D_0\rightarrow{}^7F_1$ transition is the second-most intense transition, which is a magnetic-dipole transition and independent of the coordination sphere. The intensity ratio of the $^5D_0\rightarrow{}^7F_2$ transition and the $^5D_0\rightarrow{}^7F_1$ transition is a measure for the symmetry of the coordination sphere.[36,37] For **3a**, the $^7F_2$/$^7F_1$ intensity ratio is equal to 3.8. An intensity ratio of 0.67 was reported for centrosymmetric $Eu^{III}$ complexes, whilst the $^7F_2$/$^7F_1$ intensity ratio ranges from 8 to 12 for an asymmetric coordination sphere.[36,37]

The emission spectrum of **4** displays typical band features originating from the transition of the $^5D_4$ ground state to the $^7F_J$ multiplets (Figure 6). The dominant peak is the hypersensitive transition $^5D_4\rightarrow{}^7F_5$, which is made up of a single intense peak at 545 nm. The bands at 490, 584, and 623 nm are attributed to the transitions from the $^5D_4$ state to $^7F_6$, $^7F_4$, and $^7F_3$; these transitions have medium intensity and show moderate sensitivity to the ligand environment.[38,39] The excitation spectra of **3a** and **4** exhibit the highest intense band at 267 nm that matches the absorption spectra, which confirms that the energy transfer takes place from the ligand to the rare-earth ion. Although the resolution of the spectra precludes a detailed analysis of the symmetry of the complexes, it is noteworthy that the features observed in the emission spectra of $Eu^{III}$ and $Tb^{III}$ do not

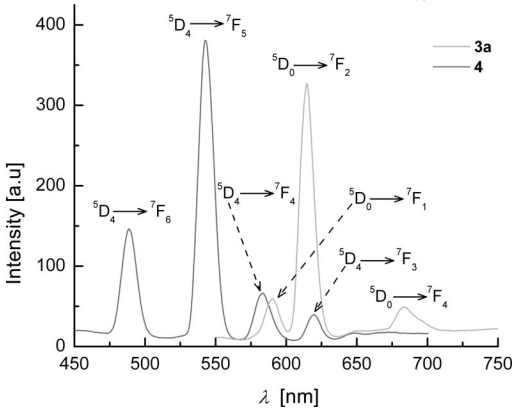


Figure 6. The emission spectra ($\lambda_{exc}$ = 275 nm) of complexes **3a** and **4**.

change upon varying the number of water lattice molecules. This result indicates that the water molecules are not present in the first coordination sphere and the metal center is not exposed to direct potential interaction with the water molecules.

## Magnetic Properties

Temperature-dependent magnetic susceptibility data of the compacted polycrystalline samples of **1**, **2a**, **3a**, and **4** were measured in the 4–300 K temperature range in a 0.1 T magnetic field. All the rare-earth(III) ions reported in this study have orbitally degenerate ground states, which are split by spin–orbit coupling and crystal field effects. The large spin-orbit coupling partly removes the degeneracy of the $^{2S+1}L$ group term of rare-earth ions, which gives $^{2S+1}L_J$ states, which can be further split into Stark levels by crystal field perturbation. For $Pr^{III}$, $Nd^{III}$ and $Tb^{III}$, the energy separation between the $^{2S+1}L_J$ ground state and the first excited state is so large that only the ground state is thermally populated at room and low temperature.[40,41] In the case of the $Eu^{III}$ ion, the first excited state may be thermally populated because of the weak energy separation.[40,41]

For **1**, the value of the $\chi_M T$ product at 300 K is 1.55 $cm^3\,K\,mol^{-1}$, which indicates that the first excited state, $^3H_5$, is not populated at room temperature.[41] As the temperature is lowered, the value of $\chi_M T$ decreases smoothly to 0.23 $cm^3\,K\,mol^{-1}$ at 2 K (Figure 7). The temperature dependence of **1** follows the Curie–Weiss behavior in the temperature range 50–300 K; at temperatures lower than 50 K, deviation from the linear Curie–Weiss behavior was observed. Below 50 K, the magnetic susceptibility data were analyzed with a model that includes the zero-field splitting ($\Delta$) of the spin–orbit coupling magnetic energy levels (inset in Figure 7).[42,43] A least-squares fit to the data leads to $g$ = 0.69, $\Delta$ = 1.23 $cm^{-1}$, and $R = 5.8\times10^{-4}$ {$R$ is defined as $\Sigma[(\chi_M)_{obsd.} - (\chi_M)_{calcd.}]^2/\Sigma[(\chi_M)_{obsd.}]^2$}. These values are reasonably close to those reported for $Pr^{III}$ sites of low symmetry.[44]

  

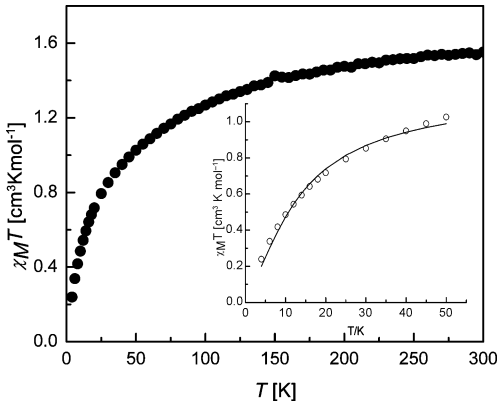


Figure 7. Temperature dependence of $\chi_M T$ for **1**. Inset: Least-square fit of the $\chi_M T$ data (open circles are the experimental data and the continuous line represents the calculated value).

The $\chi_M T$ value of **2a** is equal to 1.60 $cm^3 K mol^{-1}$ at 300 K; this value is close to that expected for the free $Nd^{III}$ ion (1.64 $cm^3 K mol^{-1}$) On lowering the temperature, $\chi_M T$ continuously decreases to a value of 0.70 $cm^3 K mol^{-1}$ at 4 K (Figure 8). The temperature dependence of $\chi_M T$ mainly depends on the populations of the Stark levels.[40,41] In the 100–300 K temperature range, the magnetic susceptibility data of **2a** can be described by a Curie–Weiss fitting with $C$ = 1.81 $cm^3 K mol^{-1}$ and $\theta$ = –38 K.

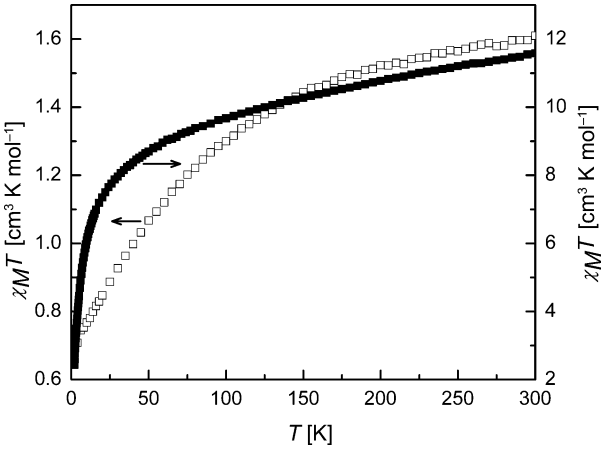


Figure 8. Temperature dependence of $\chi_M T$ for **2a** (□) and **4** (■).

In the case **3a**, the first-order magnetic moment of $Eu^{III}$ is zero due to the nonmagnetic ground state ($^7F_0$). Because the spin–orbit parameter ($\lambda$) is small enough, the first $^7F_1$ and second $^7F_2$ excited states can be thermally populated at room temperature and above. The 1.69 $cm^3 K mol^{-1}$ value of $\chi_M T$ observed in **3a** at 300 K corresponds to the population of an excited state (the theoretical value is 1.6 $cm^3 K mol^{-1}$).[45] As the temperature is lowered, the value of $\chi_M T$ decreases and is equal to 0.037 $cm^3 K mol^{-1}$ at 4 K (Figure 9), which indicates that that the $^7F_0$ ground state of the $Eu^{III}$ ions is populated in the very-low temperature range. Bellow 100 K, $\chi_M T$ versus $T$ is rigorously linear with slope $(\chi_M T)_{LT} = 7.3 \times 10^{-3}$ $cm^3 K mol^{-1}$ (inset in Figure 9). The calculated $\lambda$ value[45] leads to 285 $cm^{-1}$, which represents the energy gap between $^7F_0$ and $^7F_1$; this value is in the range of those generally observed for polynuclear $Eu^{III}$ complexes.[46–48]

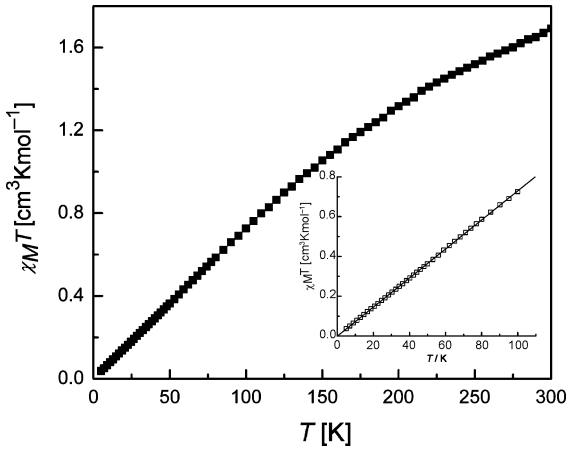


Figure 9. Temperature dependence of $\chi_M T$ for **3a**. Inset: Linear fit of $\chi_M T$ vs. $T$ in the 4–100 K temperature range.

For **4**, the $\chi_M T$ value at 300 K is equal to 11.58 $cm^3 K mol^{-1}$, which is slightly lower than the calculated value of 11.82 $cm^3 K mol^{-1}$ for the free $Tb^{III}$ ion. From 300 to 4 K, the $\chi_M T$ value decreases slowly to 2.42 $cm^3 K mol^{-1}$ (Figure 8); this behavior is typical to the depopulation of the Stark levels.[41]

## Conclusions

Rare-earth-based extended networks with the ligand 1,4-bis(pyridine-2-carboxamido)butane were synthesized and characterized by various techniques. The ligand is coordinated in a tetradentate manner and it bridges rare-earth(III) ions. The coordination number provided by the three ligand molecules coordinated to the same rare-earth ion is only six; the coordination sphere is completed by two chlorido ions and one methanol molecule to make a coordination number of nine. X-ray crystallographic studies showed that the cavities formed within the 2D structure are filled with free chloride ions and methanol molecules. The methanol molecules are replaced by water molecules when the compounds are exposed to air. The photophysical properties in the solid state reveal the presence of a single luminescent site in the complexes containing $Eu^{III}$ and $Tb^{III}$, in agreement with the crystallographic data. The temperature dependence of the magnetic susceptibility of the complexes studied is strongly dominated by the spin–orbit coupling and the crystal field effects of the corresponding rare-earth ions. Studies regarding complex formation with other counteranions and various bridging units between the two pyridine-2-carboxamide units of the ligand are underway.

  

## Experimental Section

**General Remarks:** Starting materials were purchased from Aldrich and all manipulations were performed by using the materials as received. The ligand 1,4-bis(pyridine-2-carboxamido)butane was synthesized from pyridine-2-carboxylic acid and 1,4-diaminobutane by using literature methods.[49]

**Synthesis of the Coordination Compounds:** A solution of $RECl_3 \cdot 6H_2O$ (0.12 mmol) in methanol (10 mL) was added to a solution of ligand (0.18 mmol) in methanol (5 mL). Diisopropyl ether was allowed to diffuse slowly into this solution at 4 °C, and crystals were obtained within a few days. After filtration, the crystalline material was washed with diisopropyl ether and dried in air. The complexes obtained have the general formula $[RE(L)_{1.5}Cl_2(CH_3OH)]Cl \cdot nS$ (RE = Pr **1**, Nd **2a**, Eu **3a**, Tb **4** for $n = 4$, S = $H_2O$; Nd **2b**, Eu **3b** for $n = 5$, S = $CH_3OH$).

**1:** Yield: 47% (45 mg). IR: $\tilde{\nu}$ = 3217 (br.), 3094 (m), 2981 (m), 2858 (m), 1629 (s), 1592 (s), 1557 (s), 1471 (m), 1436 (m), 1336 (m), 1307 (m), 1260 (w), 1200 (w), 1106 (m), 818 (m), 752 (m), 685 (m), 630 (m) $cm^{-1}$. $C_{25}H_{39}Cl_3N_6O_8Pr$ (798.88): calcd. C 37.59, H 4.92, N 10.52; found C 37.55, H 5.17, N 10.51.

**2a:** Yield: 58% (56 mg). IR: $\tilde{\nu}$ = 3218 (br.), 3054 (m), 2978 (m), 2860 (m), 1627 (s), 1593 (s), 1557 (s), 1472 (m), 1436 (m), 1338 (m), 1307 (m), 1260 (w), 1200 (w), 1107 (m), 818 (m), 754 (m), 684 (m), 630 (m) $cm^{-1}$. $C_{25}H_{39}Cl_3N_6NdO_8$ (802.40): calcd. C 37.42, H 4.90, N 10.47, Cl 13.26, Nd 18.00; found C 37.27, H 4.95, N 10.50, Cl 13.30, Nd 17.9.

**3a:** Yield: 54% (52 mg). IR: $\tilde{\nu}$ = 3220 (br.), 3054 (m), 2978 (m), 2861 (m), 1626 (s), 1593 (s), 1557 (s), 1473 (m), 1438 (m), 1338 (m), 1309 (m), 1260 (w), 1201 (w), 1107 (m), 818 (m), 755 (m), 684 (m), 632 (m) $cm^{-1}$. $C_{25}H_{39}Cl_3EuN_6O_8$ (809.94): calcd. C 37.07, H 4.85, N 10.38; found C 36.89, H 4.98, N 10.25.

**4:** Yield: 49% (48 mg). IR: $\tilde{\nu}$ = 3222 (br.), 3057 (m), 2976 (m), 2859 (m), 1629 (s), 1597 (s), 1557 (s), 1472 (m), 1436 (m), 1340 (m), 1308 (m), 1262 (w), 1200 (w), 1109 (m), 818 (m), 755 (m), 684 (m), 632 (m) $cm^{-1}$. $C_{25}H_{39}Cl_3N_6O_8Tb$ (816.90): calcd. C 36.76, H 4.81, N 10.29; found C 36.94, H 5.02, N 10.22.

**Physical Measurements:** C, H, and N analyses were performed with a Perkin–Elmer 2400 series II analyzer. Infrared spectra (4000–300 $cm^{-1}$, resol. 4 $cm^{-1}$) were recorded with a Perkin–Elmer Paragon 1000 FTIR spectrometer equipped with a Golden Gate ATR device by using the reflectance technique. Diffuse reflectance spectra were obtained with a Perkin–Elmer Lambda 900 spectrophotometer by using MgO as a reference. The excitation and emission spectra were recorded with a Perkin–Elmer LS50B luminescence spectrometer. The intensity of the emission spectra was corrected for the sensitivity of the detector. Magnetic susceptibility measurements (4–300 K) were carried out on polycrystalline sample at 0.1 T by using a Quantum Design MPMS-5 5T SQUID magnetometer. Data were corrected for the magnetization of the sample holder and for diamagnetic contributions, which were estimated from the Pascal constants. Thermogravimetric analysis was carried out on a Du Pont TG-DTA analyzer. Thermal analysis was carried out from room temperature to 800 °C at a heating rate of 5 °C $min^{-1}$ under an atmosphere of dioxygen with open sample holder and small platinum boat.

**X-ray Crystallographic Analysis and Data Collection:** Intensity data for a single crystals of **2b** and **3b** were collected by using Mo-$K_\alpha$ radiation ($\lambda$ = 0.71073 Å) with a Nonius KappaCCD diffractometer. The intensity data were corrected for Lorentz and polarization effects, for absorption (ψ-scan absorption correction), and extinction. The structures were solved by direct methods. The programs COLLECT,[50] SHELXS-97,[51] and SHELXL-97[52] were used for data reduction, structure solution, and structure refinement, respectively. Refinement of $F^2$ was done against all reflections. The weighted $R$ factor, $wR$, and goodness of fit $S$ are based on $F^2$. Conventional $R$ factors are based on $F$, with $F$ set to zero for negative $F^2$. All non-hydrogen atoms were refined with anisotropic displacement parameters. All hydrogen atoms were introduced in calculated positions and refined with fixed geometry with respect to their carrier atoms. Crystal and refinement data for **2b** and **3b** are shown in Table 2. CCDC-658469 (for **2b**) and -658470 (for **3b**) contain the supplementary crystallographic data for this paper. These data can be obtained free of charge from The Cambridge Crystallographic Data Centre via www.ccdc.cam.ac.uk/data_request/cif.

Table 2. Crystal data and details of the structure determinations for **2b** and **3b**.

| | **2b** | **3b** |
|---|---|---|
| Formula | $C_{30}H_{51}Cl_3N_6NdO_9$ | $C_{30}H_{51}Cl_3EuN_6O_9$ |
| Formula weight | 890.36 | 898.08 |
| Crystal system | monoclinic | monoclinic |
| Space group | $P2_1/n$ (no 14) | $P2_1/n$ (no 14) |
| $a$ [Å] | 14.389(3) | 14.218(3) |
| $b$ [Å] | 20.419(4) | 20.364(4) |
| $c$ [Å] | 15.101(3) | 14.988(3) |
| $\alpha$ [°] | 90 | 90 |
| $\beta$ [°] | 105.81(3) | 106.11(3) |
| $\gamma$ [°] | 90 | 90 |
| $V$ [Å$^3$] | 4269.0(16) | 4169.1(16) |
| $Z$ | 4 | 4 |
| $D_{calcd.}$ [mg m$^{-3}$] | 1.385 | 1.431 |
| $\mu$ (Mo-$\alpha$) [mm$^{-1}$] | 1.454 | 1.748 |
| Crystal size [mm] | 0.15 × 0.30 × 0.35 | 0.15 × 0.30 × 0.35 |
| $T$ [K] | 173(2) | 173(2) |
| Data collected | 47613 | 49070 |
| Unique data | 8196 | 8116 |
| $R_{int}$ | 0.078 | 0.088 |
| $R(F)$ [$I > 2\sigma(I)$] | 6007 | 5504 |
| $wR(F^2)$ | 0.0554 | 0.0554 |
| $S$ | 1.12 | 1.06 |
| $\Delta\rho_{min}$, $\Delta\rho_{max}$ [e Å$^{-3}$] | –1.52, 2.73 | –1.02, 3.24 |

**Supporting Information** (see footnote on the first page of this article): Degradation stages and weight loss of **1** and **2a**.

## Acknowledgments

This research was supported by a Veni grant from the Netherlands Organization for Scientific Research (NWO) to S. T. and the Leiden University Study group WFMO (Werkgroep Fundamenteel Materialen Onderzoek).

[1] M. N. Bochkarev, *Chem. Rev.* **2002**, *102*, 2089–2117.
[2] N. Ishikawa, M. Sugita, T. Ishikawa, S. Koshihara, Y. Kaizu, *J. Am. Chem. Soc.* **2003**, *125*, 8694–8695.
[3] J. Kido, Y. Okamoto, *Chem. Rev.* **2002**, *102*, 2357–2368.
[4] N. Marques, A. Sella, J. Takats, *Chem. Rev.* **2002**, *102*, 2137–2159.
[5] S. Petoud, S. M. Cohen, J. C. G. Bunzli, K. N. Raymond, *J. Am. Chem. Soc.* **2003**, *125*, 13324–13325.
[6] J. K. Tang, I. Hewitt, N. T. Madhu, G. Chastanet, W. Wernsdorfer, C. E. Anson, C. Benelli, R. Sessoli, A. K. Powell, *Angew. Chem. Int. Ed.* **2006**, *45*, 1729–1733.

  

[7] C. M. Zaleski, E. C. Depperman, J. W. Kampf, M. L. Kirk, V. L. Pecoraro, *Angew. Chem. Int. Ed.* **2004**, *43*, 3912–3914.
[8] M. Eddaoudi, H. L. Li, T. Reineke, M. Fehr, D. Kelley, T. L. Groy, O. M. Yaghi, *Top. Catal.* **1999**, *9*, 105–111.
[9] Z. Y. Li, G. S. Zhu, X. D. Guo, X. J. Zhao, Z. Jin, S. L. Qiu, *Inorg. Chem.* **2007**, *46*, 5174–5178.
[10] J. Xia, B. Zhao, H. S. Wang, W. Shi, Y. Ma, H. B. Song, P. Cheng, D. Z. Liao, S. P. Yan, *Inorg. Chem.* **2007**, *46*, 3450–3458.
[11] J. G. Mao, *Coord. Chem. Rev.* **2007**, *251*, 1493–1520.
[12] Y. G. Huang, B. L. Wu, D. Q. Yuan, Y. Q. Xu, F. L. Jiang, M. C. Hong, *Inorg. Chem.* **2007**, *46*, 1171–1176.
[13] P. Mahata, S. Natarajan, *Inorg. Chem.* **2007**, *46*, 1250–1258.
[14] X. Y. Chen, Y. Bretonniere, J. Pecaut, D. Imbert, J. C. Bunzli, M. Mazzanti, *Inorg. Chem.* **2007**, *46*, 625–637.
[15] S. Tanase, F. Prins, J. M. M. Smits, R. de Gelder, *Crystengcomm* **2006**, *8*, 863–865.
[16] S. C. Manna, E. Zangrando, A. Bencini, C. Benelli, N. R. Chaudhuri, *Inorg. Chem.* **2006**, *45*, 9114–9122.
[17] X. D. Guo, G. S. Zhu, F. X. Sun, Z. Y. Li, X. J. Zhao, X. T. Li, H. C. Wang, S. L. Qiu, *Inorg. Chem.* **2006**, *45*, 2581–2587.
[18] C. Qin, X. L. Wang, E. B. Wang, Z. M. Su, *Inorg. Chem.* **2005**, *44*, 7122–7129.
[19] A. Michaelides, S. Skoulika, *Cryst. Growth Des.* **2005**, *5*, 529–533.
[20] S. K. Ghosh, P. K. Bharadwaj, *Inorg. Chem.* **2004**, *43*, 2293–2298.
[21] J. Rocha, L. D. Carlos, *Curr. Opin. Solid State Mater. Sci.* **2003**, *7*, 199–205.
[22] R. J. Hill, D. L. Long, P. Hubberstey, M. Schroder, N. R. Champness, *J. Solid State Chem.* **2005**, *178*, 2414–2419.
[23] R. J. Hill, D. L. Long, N. R. Champness, P. Hubberstey, M. Schroder, *Acc. Chem. Res.* **2005**, *38*, 335–348.
[24] D. L. Long, A. J. Blake, N. R. Champness, C. Wilson, M. Schroder, *Chem. Eur. J.* **2002**, *8*, 2026–2033.
[25] D. L. Long, A. J. Blake, N. R. Champness, C. Wilson, M. Schroder, *Angew. Chem. Int. Ed.* **2001**, *40*, 2443–2447.
[26] D. L. Long, A. J. Blake, N. R. Champness, M. Schroder, *Chem. Commun.* **2000**, 1369–1370.
[27] A. Scarso, J. Rebek Jr, in *Topics in Current Chemistry Vol 265: Supramolecular Chirality* (Eds.: M. Crego-Calama, D. N. Reinhoudt), Springer, Berlin, **2006**, vol. 265, pp. 1–46.
[28] G. Seeber, B. E. F. Tiedemann, K. N. Raymond in *Topics in Current Chemistry Vol 265: Supramolecular Chirality* (Eds.: M. Crego-Calama, D. N. Reinhoudt), Springer, Berlin, **2006**, pp. 147–183.
[29] T. K. Ronson, H. Adams, L. P. Harding, S. J. A. Pope, D. Sykes, S. Faulkner, M. D. Ward, *Dalton Trans.* **2007**, 1006–1022.
[30] H. Masu, M. Tominaga, K. Katagiri, T. Kato, I. Azumaya, *Crystengcomm* **2006**, *8*, 578–580.
[31] K. L. Wong, G. L. Law, W. M. Kwok, W. T. Wong, D. L. Phillips, *Angew. Chem. Int. Ed.* **2005**, *44*, 3436–3439.
[32] S. Tanase, P. M. Gallego, R. de Gelder, W. T. Fu, *Inorg. Chim. Acta* **2007**, *360*, 102–108.
[33] K. Nakamoto, *Infrared and Raman Spectra of Inorganic and Coordination Compounds*, 3rd ed., John Wiley, New York, **1978**.
[34] E. Antic-Fidancev, F. Serpaggi, G. Ferey, *J. Alloys Compd.* **2002**, *340*, 88–94.
[35] G. Oczko, J. Legendziewicz, M. S. Wickleder, G. Meyer, *J. Alloys Compd.* **2002**, *341*, 255–262.
[36] A. F. Kirby, F. S. Richardson, *J. Phys. Chem.* **1983**, *87*, 2544–2556.
[37] A. F. Kirby, D. Foster, F. S. Richardson, *Chem. Phys. Lett.* **1983**, *95*, 507–512.
[38] F. S. Richardson, *Chem. Rev.* **1982**, *82*, 541–552.
[39] F. S. Richardson, *Chem. Phys. Lett.* **1982**, *86*, 47–50.
[40] R. L. Carlin, *Magnetochemistry*, Springer, Berlin, **1997**.
[41] O. Kahn, *Molecular Magnetism*, VCH, **1993**.
[42] I. A. Kahwa, J. Selbin, C. J. O'Connor, J. W. Foise, G. L. McPherson, *Inorg. Chim. Acta* **1988**, *148*, 265–272.
[43] C. J. O'Connor, *Progr. Inorg. Chem.* **1982**, *29*, 203–283.
[44] V. E. Sells, D. Bloor, *J. Phys. C - Solid State Phys.* **1976**, *9*, 379–387.
[45] M. Andruh, E. Bakalbassis, O. Kahn, J. C. Trombe, P. Porcher, *Inorg. Chem.* **1993**, *32*, 1616–1622.
[46] J. Legendziewicz, M. Borzechowska, *J. Alloys Compd.* **2000**, *300*, 353–359.
[47] J. Legendziewicz, V. Tsaryuk, V. Zolin, E. Lebedeva, M. Borzechowska, M. Karbowiak, *New J. Chem.* **2001**, *25*, 1037–1042.
[48] Y. Li, F. K. Zheng, X. Liu, W. Q. Zou, G. C. Guo, C. Z. Lu, J. S. Huang, *Inorg. Chem.* **2006**, *45*, 6308–6316.
[49] D. J. Barnes, R. L. Chapman, R. S. Vagg, E. C. Watton, *J. Chem. Eng. Data* **1978**, *23*, 349–350.
[50] *COLLECT*, Nonius BV, Delft, The Netherlands, **2002**.
[51] G. M. Sheldrick, *SHELXS-97*, University of Göttingen, Germany, **1997**.
[52] G. M. Sheldrick, *SHELXL-97*, University of Göttingen, Germany, **1997**.

Received: January 12, 2008
Published Online: March 20, 2008

  